ACS APPLIED MATERIALS & INTERFACES

Research Article

Cite This: ACS Appl. Mater. Interfaces 2019, 11, 35305−35311

www.acsami.org

Delignified Wood−Polymer Interpenetrating Composites Exceeding the Rule of Mixtures

M. Frey,*[,†,§] L. Schneider,[†,§] K. Masania,[‡] T. Keplinger,*[,†,§] and I. Burgert[†,§]

[†]Wood Materials Science, Institute for Building Materials, and [‡]Complex Materials, Department of Materials, ETH Zürich, CH-8093, Zurich, Switzerland

[§]WoodTec Group, Cellulose & Wood Materials, EMPA, CH-8600, Dübendorf, Switzerland

Supporting Information

ABSTRACT: Wood is increasingly considered in sustainable structural materials development due to its hierarchical structure, including an oriented reinforcing cellulose phase combined with carbon capturing and renewability. Top-down manufacturing techniques can provide direct access to this hierarchical cellulose scaffold for use in new functional materials. For high-performance load-bearing wood-based materials, the volume content of the reinforcing phase needs to be increased to much higher fiber volume contents (FVCs). This has been achieved by structure-retaining delignification followed by densification. The obtained matrix-free materials possess high tensile stiffness due to preservation of hierarchical fiber alignment; however, they demonstrate low mechanical properties in bending and cannot be used in moist conditions due to their propensity for water absorption. In order to address these two challenges, an interpenetrating wood polymer phase composite is developed using a delignified wood scaffold as a continuous reinforcing phase and epoxy resin as the interconnected matrix phase. We utilize the continuous flow channels in delignified wood for vacuum-assisted matrix infiltration in a condition of open continuous porosity in the wood scaffold. Prior to matrix curing, the material is densified in order to increase the FVC, decrease porosity, and reduce density variations in the wood scaffold. Due to the compressibility of delignified cellulose fibers, interpenetrating phase composites (IPCs) with very high FVCs of up to 80% could be produced, leading to exceptionally high tensile stiffness and strength of up to 70 GPa and 600 MPa. The obtained stiffness values far exceed the upper limit of the rule of mixtures due to an enhanced stress transfer through mechanically interlocked fiber−fiber interfaces combined with the stiffness providing matrix phase that further aids stress transfer between neighboring wood cells via their pits. This new approach paves the way for an efficient production of high-performance sustainable materials that can be used as alternative for glass fiber reinforced composites or natural fiber composites.

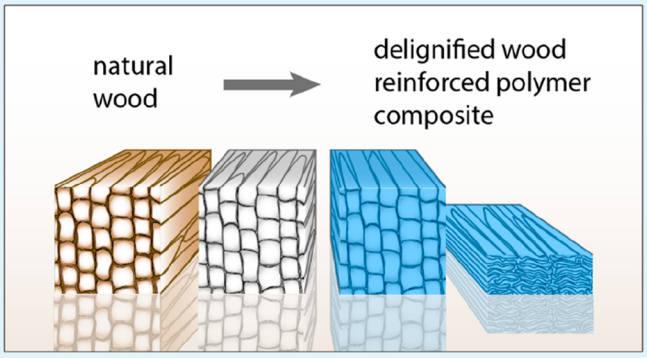

KEYWORDS: *interpenetrating composites, natural fiber composites, high fiber volume content, cellulose scaffold densification, glass fiber alternative*

INTRODUCTION

In view of depleting resources and rising emissions of greenhouse gases, there is a fast-growing need to replace synthetic engineering materials by renewable materials.[1−3] Wood is a key material for a transition to sustainable societies and economies because it is biobased and captures CO_2 during growth. Today, wood is readily available in large volumes at low cost, and it combines good mechanical performance with a lightweight design due to a structural optimization toward mechanical stiffness, strength, and porosity for water transport in the living tree. However, there are still certain limitations for wood-based materials when it comes to high-end structural applications. Limitations mainly occur because of modest mechanical performance arising from the tree's optimization for both functions, support and flow conductivity, and from low reliability caused by the heterogeneity of the natural material.[4]

Functional wood-based materials have been manufactured either by deconstructing wood into smaller pieces and assembling the obtained building blocks in a new architecture in a bottom-up approach[5−7] or by direct utilization of the reinforcing cellulose scaffolds after wood modification in a top-down approach.[8] Deconstruction of wood followed by reassembly eliminates inhomogeneities, but it can be difficult to achieve targeted performances in a scalable and efficient way. The top-down approach, aiming at modification and utilization of the hierarchical wood structure, has recently

Received: June 25, 2019
Accepted: August 27, 2019
Published: August 27, 2019

DOI: 10.1021/acsami.9b11105
ACS Appl. Mater. Interfaces 2019, 11, 35305−35311

gained importance as it enables the fabrication of wood-based materials with excellent mechanical properties[9,10] and novel functionalities such as transparency,[11,12] magnetism,[13,14] insulation,[15] or filtering applications.[16]

Wood-based cellulose scaffolds are obtained by structure-preserving delignification of wood followed by drying in a scalable top-down manufacturing process. After full delignification and drying, neighboring fibers come into close contact to one other, building an interconnected cellulose phase, enabling stress transfer in the scaffold, even without the need of a matrix.[17] The resulting lightweight cellulose scaffolds can further be densified in order to obtain a very stiff and strong cellulose bulk material.[9,17] Alternatively, Song et al. investigated partially delignified wood scaffolds that were densified by hot-pressing to utilize the remaining lignin as matrix and achieved excellent mechanical performance.[10] However, partial delignification of bulk wood can lead to compositional inhomogeneities and gradients within the scaffold and the cell walls (Figure S1),[17] which can be avoided by complete lignin removal. Both partial and complete lignin removal lead to enhanced exposure of the hydrophilic cellulose, which results in an even more pronounced influence of humidity on mechanical properties compared to natural wood.[17,18] Subsequently, exposure of densified wood material to water leads to relaxation of internal stresses and partial thickness recovery, also referred to as spring-back effect.[19] Coatings or polymer infiltration can reduce the influence of moisture and can enhance structural integrity.[17] Yano et al. obtained moisture-stable, very stiff, and very strong wood-based composites by delignification of carefully preselected wood based on stiffness grading followed by phenolic resin (PF resin) infiltration and densification.[20−23] However, the need of preselection combined with relatively long infiltration times reduces scalability of this approach.

To address some of these challenges, we fabricate an interpenetrating wood polymer phase composite by structure-retaining delignification of spruce wood followed by an efficient vacuum-assisted polymer infiltration and densification (Figure 1). Using the inherent transportation path through lumina and pits, infiltration of a continuous matrix phase results in a complex flow behavior that leads to an interpenetrating phase composite. Densification in the infiltrated state before curing allows the simultaneous reduction of density variations and increasing of the fiber volume content (FVC) in the wood scaffold resulting in very high stiffness and strength in an efficient approach and without preselection of specimens.

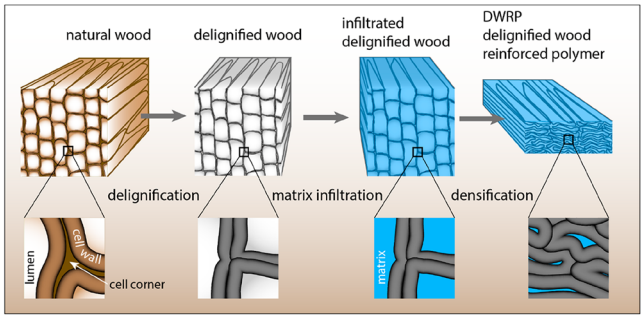

Figure 1. Schematic illustrating the fabrication of delignified wood reinforced polymer (DWRP) composites. Natural wood is delignified, resulting in a continuous open porous structure that can be infiltrated with a polymer matrix and densified to a desired fiber volume content (FVC). The combination of mechanical interlocks and bicontinuous phase structure allows for stress transfer in the composite.

EXPERIMENTAL SECTION

Delignified Wood. For obtaining the cellulose scaffolds, Norway spruce (*Picea abies*) samples with the dimensions 100 × 20 × 10 mm^3 and 100 × 20 × 5 mm^3 (longitudinal *x* tangential *x* radial) were delignified for 2 × 6 h following the protocol reported in Frey et al.,[9] and Segmehl et al.[24] Wood samples are placed into a beaker on top of a metal-grid sample holder, and an equal-volume mixture of hydrogen peroxide solution (35 wt %, Acros Organics) and glacial acetic acid (Fisher Chemicals) was poured into the beaker. After infiltration overnight at room temperature (RT) under stirring, the solution was heated, and the wood pieces were delignified for 6 h at 80 °C. The obtained cellulose scaffolds were washed in deionized water until a pH value above 5 was reached, and then the samples were conditioned at 65% RH/20 °C.

Infiltration of Matrix. The cellulose scaffolds were dried in an oven at 65 °C overnight. The dry cellulose scaffolds were then infiltrated with the epoxy resin system RIM 235/RIMH 238 (Hexion, U.S.A.) by vacuum-assisted resin infusion (VARI). The infusion resin system was chosen due to its low viscosity (1000−1300 mPa·s) combined with a long pot life (>10 h). The epoxy resin and hardener were mixed at a weight ratio of 100:34, stirred, and then degassed in a vacuum oven for 15 min. The VARI setup, illustrated in Figure S2, was built as follows: Three cellulose scaffolds were placed on a steel plate. A net bleeder (Suter Kunststoffe, Switzerland) was placed between the inlet and the sample, and a breather cloth (Suter Kunststoffe, Switzerland) surrounded the cellulose scaffolds for an eased air flow. Spiral tubes surrounded by breather cloth were used at the inlet and outlet to allow for degassing. A rather long distance between scaffolds and outlet of 22 cm was chosen in order to generate a slow flow front of the epoxy, reducing porosity during infiltration of the scaffold. The vacuum bag was sealed using tacky tape (Suter Kunststoffe, Switzerland), and the outlet was connected to the vacuum pump (CVC 3000, Vacuumbrand, Germany). Inlet and outlet were regulated with clamps, and the infiltration of the cellulose scaffolds was conducted for 90 min.

Densification. Densification was conducted in a compression resin transfer mold (CRTM)[25] with three cavities to densify three infiltrated samples at the same time under an isostatic pressure and to obtain FVCs ranging from 25% up to 80% depending on the mold spacing. Prior to densification, the mold was coated with release agent (Loctite 770-NC Frekote, Henkel, Germany) and the edges were additionally greased with a Motorex lithium grease. A 0.05 mm thick Teflon foil was placed between samples and stamp to ease the release of the samples after densification. Samples were placed into the mold, and additional epoxy was poured into the mold until a total weight of 50 g of epoxy per mold was reached in order to have a constant amount of epoxy. The infiltrated scaffolds were densified using a LabEcon (Fontijn, Netherlands) hot press for 5 h at 60 °C at a pressure of approximately 3 bar. The thickness of the samples after densification was regulated using aluminum spacers between the press and the mold surface.

Glass Fiber Reinforced Polymer (GFRP) Reference Samples. Samples were manufactured by compression resin transfer molding. A unidirectional (UD) glass fiber fabric, 220 g/m^2 (Suter Kunststoffe, Switzerland), was cut to 150 × 90 mm^2 using a digital cutter G3M2500 (Zünd, Switzerland). An amount of 30 g of epoxy and 15 or 8 GF layers were used to produce 50% or 25% FVC composites, respectively. The GFRP reference samples were densified under the same conditions as described for delignified wood reinforced polymer (DWRP) but in a simple CRTM mold with a flat stamp. Densification and curing was conducted as with the DWRP samples. The FVC of the GFRP samples was determined by ignition loss of cured resin in accordance with ASTM D2584.

Tensile and Three-Point Bending Testing. The samples were cut to the dimensions of 100 × 20 × 2.5 mm^3 for tensile testing and

DOI: 10.1021/acsami.9b11105
ACS Appl. Mater. Interfaces 2019, 11, 35305−35311

100 × 12.7 × 2.5 mm^3 for bending testing using a circular saw (Proxxon, Luxembourg). The clamping area of the tensile samples was reinforced with 2 mm thick GF plates (Suter Kunststoffe, Switzerland). DWRPs with FVCs of approximately 25%, 50%, and 70% were tested in tension and bending using eight samples per batch. Before tensile testing, samples were conditioned at 65% RH and 20 °C until constant mass was obtained. Tensile properties were determined using a universal testing machine (ZwickRoell, Germany) equipped with a 100 kN load cell at 20 °C and 65% RH in accordance to ISO 527 with an initial clamp distance of 46 mm and a crosshead speed of 5 mm/min. The change in length was measured with a contact extensometer (ZwickRoell, Germany) with an initial length of 20 mm.

Three-point bending measurements were used to determine the bending properties of the DWRPs using the universal testing machine, equipped with a 1 kN load cell with a crosshead speed of 4 mm/min. In accordance with ASTM D790, the span between the loading supports was set to 80 mm, which results in a span-to-thickness ratio of approximately 32, and the radii of the loading nose and loading supports were chosen to be 5 and 2 mm, respectively.

Microscopy and Water Uptake. Light-microscope imaging (Olympus BX51, Japan), scanning electron microscopy (SEM) imaging (Hitachi SU5000, Japan), and atomic force microscopy (AFM) imaging (NanoWizard 4, JPK Instruments AG, Germany) were conducted in order to investigate the infiltration and densification behavior. Cross section cuts as well as longitudinal cuts (radial) were analyzed by light microscopy and SEM. DWRPs were embedded in epoxy potting resin (EpoFix, Struers GmbH, Germany), and the embedded samples were polished after curing using a LaboPol-25 (Struers GmbH, Germany). High-quality surfaces for AFM imaging were obtained using an ultramicrotome (Ultracut, Reichert-Jung, Germany) with a diamond trim knife (Diatome, Switzerland). AFM imaging was conducted in the quantitative imaging mode at 20 °C and 65% relative humidity using a noncontact cantilever (NCHR, Nano World, Switzerland). A set point of 60 nN, *z*-length of 150 nm, and a pixel time of 12 ms was used. The JPK image processing software (JPK Instruments AG) was used to process the images.

For water uptake measurements the initial mass of DWRP 70% samples was determined after oven-drying at 65 °C for 72 h, and then the samples were placed into water with slight stirring for 48 h. After water soaking the mass of the samples was again measured.

RESULTS AND DISCUSSION

Delignification of bulk wood represents a simple top-down approach to manufacture lightweight cellulose scaffolds that are composed of aligned fibers (tracheids). Lignin removal takes place in between neighboring cells and in the cell walls, which leads to an almost complete removal of the middle lamella and results in a higher porosity of the cell walls in wet state. Upon drying, the delignified wood cell walls shrink and neighboring cells get in close contact to each other, leading to cell deformation. This deformation generates wrinkled interfaces, which can act as mechanical interlocks between the cells.[17] These interlocks provide remarkable structural integrity and are responsible for the high mechanical stability even for dry cellulose scaffolds without any resin matrix.[9,17] Additionally, during structure-preserving delignification the cavities in wood cells called lumina are retained. Presumably, interconnections between lumina of neighboring cells are even improved by the partial degradation of bordered pits.[26] This percolating path can be exploited for matrix infiltration into the cellulose scaffold by vacuum-assisted resin infiltration and allows the infiltration of a hydrophobic matrix into the hydrophilic cellulose scaffold by use of Darcy-driven flow combined with capillary pressure of the small flow channels.

To investigate in detail the hydrophobic matrix infiltration through the interconnected path of the pores, radial cuts and cross sections of partially infiltrated and fully infiltrated samples were analyzed by light microscopy. The infiltration behavior observed for the radial cut (Figure 2b) appears to be

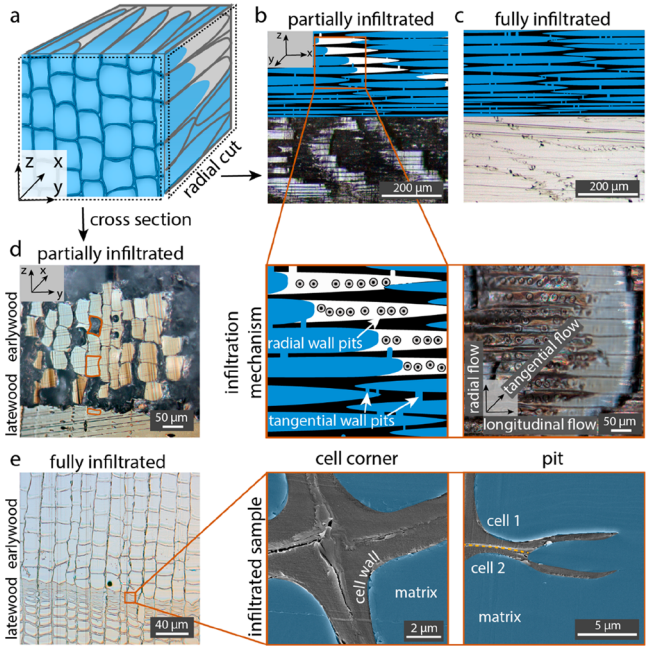

Figure 2. Light-microscopy and SEM images show the complex infiltration behavior in the wood scaffold. (a) Schematic of a delignified wood cube during infiltration along the main longitudinal *x*-axis. (b) Illustration and light-microscope image of a partially infiltrated radial cut show multiple staircase-like infiltrations taking place and zoom into region of interest to illustrate the infiltration mechanism. Bordered pits in tangential walls enable a radial flow (*y*), whereas the bordered pits in the radial wall allow the flow in tangential direction (*z*) from one cell to the other. (c) Illustration and light-microscope image of a radial cut of a fully infiltrated sample. (d) Cross section of a partially infiltrated sample shows infiltrated latewood cells (small lumen, thick cell walls) and partial infiltration of earlywood cells (large lumen, thin cell walls). (e) Cross section of a fully infiltrated sample and zoom showing structural details proving the infiltration mechanism through lumina and bordered pits: SEM image of a cell corner showing the collapsed middle lamella region, which is not filled with epoxy and SEM image of an infiltrated bordered pit.

due to simultaneous infiltration in longitudinal, radial, and tangential directions. Part of the matrix filling the lumen in the longitudinal direction flows through pits in the tangential walls, which causes a cascaded flow to neighboring cells in the radial direction. At the same time, radial wall pits allow the matrix to spread into neighboring cells in the tangential direction, which results in multiple staircase-like flow fronts. This staircase-like infiltration pattern was found in all regions of the wood, irrespective of the size of the cell lumina: small lumina of cells grown towards the end of the season (latewood tracheids), large lumina of cells grown in the early part of the season (earlywood tracheids), and cells with medium lumen size (transition wood tracheids), which form the majority of the microstructure in spruce.

Observing partially infiltrated sample cross sections to better understand the flow behavior (Figure 2d) suggests that the infiltration in latewood is faster than in earlywood. This can be

DOI: 10.1021/acsami.9b11105
ACS Appl. Mater. Interfaces 2019, 11, 35305−35311

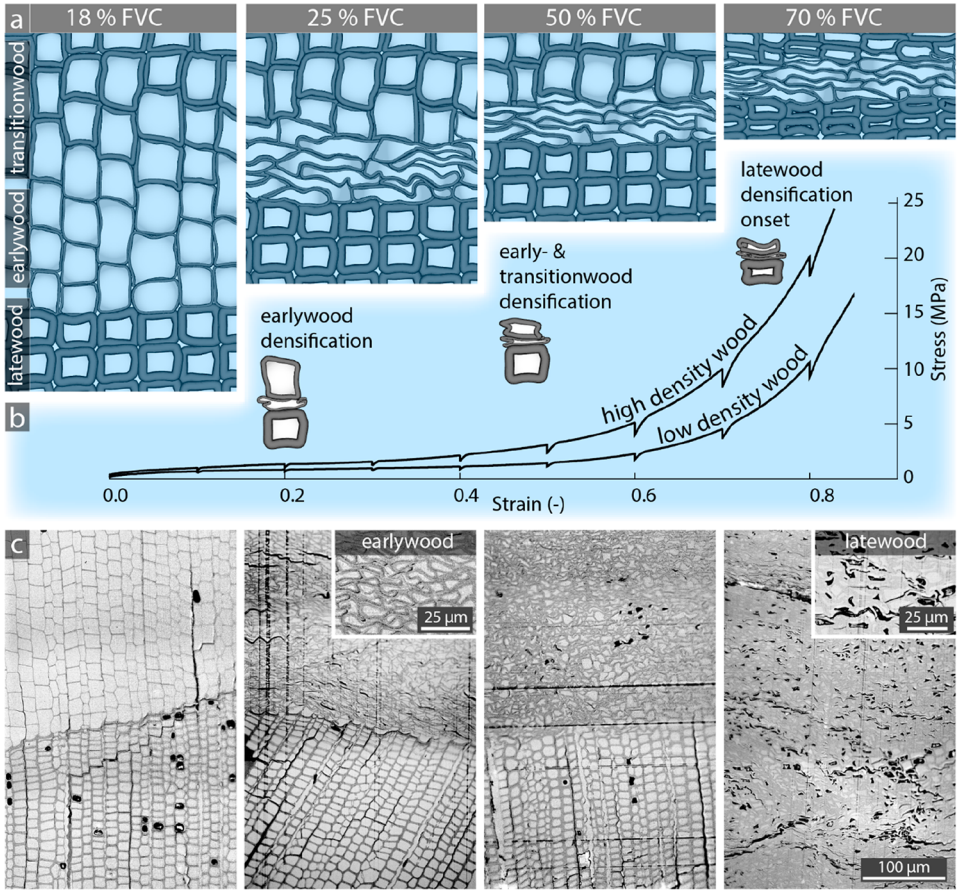

Figure 3. (a) Schematic of the densification of infiltrated samples to diferent FVCs. (b) Densification curves of cellulose scaffolds conditioned at 65% RH with high (0.38 g cm^{-3}) and low (0.27 g cm^{-3}) densities. (c) Light-microscope images of DWRP with FVCs ranging from 18% (no densification) up to 70% FVC. The thin-walled earlywood cells start folding at low densification forces (1−2 MPa), whereas transition wood and the thick-walled latewood require higher densification forces.

explained by the smaller cross sections of latewood lumina compared to earlywood.[27] The capillary pressure is indirectly proportional to the capillary diameter, which results in a higher capillary pressure to promote filling of latewood. However, the epoxy flow also depends on the applied vacuum, which leads to a mixture of capillary flow and pressure-driven Darcy flow.

The infiltration finally leads to an infiltrated three-dimensionally interconnected matrix phase (Figure 2, parts c and e). Only some minor voids and small air bubbles were visible as a result of the heterogeneity in permeability of the scaffold and the resulting race-tracks flow. Zooming into the infiltrated cross section by SEM (Figure S4) reveals that infiltration only took place in cell lumina and pits and that the interface between cells and the cell corner regions was not penetrated by the matrix. Therefore, the interaction between neighboring fibers is a combination of close contact between cell walls and their mechanical interlocking in the former middle lamella and cell corner regions as previously observed for noninfiltrated scaffolds[17] and the through pits interconnected polymer phase.

The ratio of reinforcing cellulose phase to matrix phase is increased upon densification. Figure 3a illustrates the densification of matrix-infiltrated delignified wood prior to matrix curing. We adjusted the FVC by varying the final thickness of the composite to achieve values of FVC between 18% without densification and up to 70−80% for highly densified samples, depending on the initial density of the sample. The high pressures during isostatic pressing in the CRTM mold allowed the elimination of air bubbles in the epoxy and full infiltration of the scaffold.

To investigate cell folding patterns during densification, we densified noninfiltrated delignified wood scaffolds of different densities in steps and analyzed the corresponding stress−strain curves (Figure 3b and Figure S3). Density differences of delignified wood correspond to different earlywood, transition wood, and latewood ratios within the wood sample and influence the densification. First, there is a plateau at low densification forces (1−2 MPa), corresponding to the densification of thin-walled earlywood cells. Then, the force constantly increases upon densification of transition wood (>5 MPa) and finally latewood (>10 MPa). This is due to lower thickness of earlywood cell walls compared to latewood cell walls and their larger cell diameter.[27] It follows that a high-density scaffold typically contains a lower earlywood content and requires higher densification forces at lower strain than a scaffold with a low density as shown by the densification curves of a high-density (0.38 g cm^{-3}) and a low-density (0.27 g cm^{-3}) delignified wood scaffold (Figure 3b and Figure S3). Sharp transitions in the densification force between earlywood, transition wood, and latewood are not observed due to a gradual change in density and due to mixed-mode buckling behavior depending on the thickness of the cell wall and on the loading condition. Pure Euler buckling would estimate up to 6 times higher force needed to buckle the latewood cells for the same buckling mode or 1.66 times higher force for a higher

DOI: 10.1021/acsami.9b11105
ACS Appl. Mater. Interfaces 2019, 11, 35305−35311

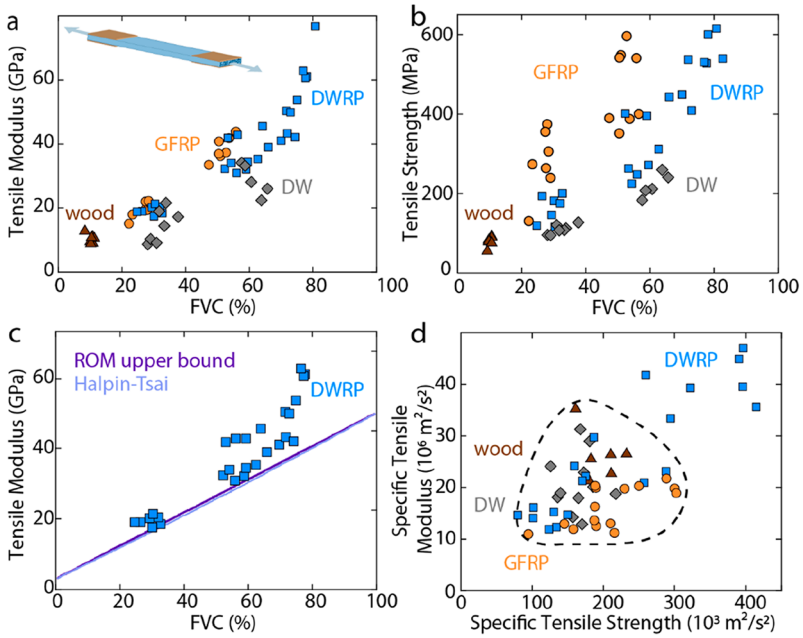

Figure 4. Tensile properties of DWRPs compared to native wood, delignified wood (DW), and glass fiber reinforced polymer (GFRP) composites. (a) Tensile modulus and (b) tensile strength of the composites as a function of their relative FVC. (c) Rule of mixture (ROM) and Halpin−Tsai models compared to the experimental tensile moduli of DWRP demonstrate that their modulus exceeds the bounds of theoretical predictions. (d) Specific tensile modulus vs specific tensile strength for comparing the density-normalized properties of the studied composites.

earlywood buckling mode (see the Supporting Information, Methods section).

Polished cross sections of DWRP at varying FVCs (Figure 3c) show a folding pattern that is similar to noninfiltrated delignified wood samples that were previously observed.[9,17] With our new approach, it is possible to manufacture DWRPs with FVCs up to 70−80%. This is beyond the practical maximum fiber content of fiber-reinforced composites, which is theoretically 70% and practically around 63−65%,[28] usually even lower for plant fiber reinforced composites due to their irregular shape.[29] In contrast to traditional plant fiber composites (e.g., flax, sisal), the polymer matrix in DWRPs fills the luminal cavities and the pits, while the outer fiber surface is in close contact to the outer surface of the neighboring fiber.

Processing of very high FVC samples above 80% is still challenging, as the cellulose scaffold starts to deform in shear. This can lead to deviations in fiber alignment from the unidirectional fiber arrangement of the scaffold. Some process-related cracking of the sample can be observed at lower FVCs as shown in Figure 3, and the light-microscope image of a polished surface of a 50% FVC DWRP (Figure S4a) reveals some cracks that may have been caused by polishing or by shrinkage of the matrix during curing. It is interesting to note that cracks are mainly present at the fiber−fiber interface of neighboring cells, resulting in fiber bridging, or in the cell walls as shown in Figure S4b. This suggests a good interfacial adhesion between the epoxy and the cell wall. Zooming into a fiber−matrix interface by SEM (Figure S4c) further shows a wrinkled interface (dashed line) caused by the densification and wrinkling of the cell wall. AFM imaging (Figure S4d) reveals an additional wrinkling at the nanometer scale.

To investigate the influence of the FVCs on the mechanical properties of DWRPs, tensile and bending tests were conducted on samples with FVCs around 25%, 50%, and 70%. The results were compared to reference materials including native wood, delignified wood (DW), and GFRP composites. High FVCs of 70% and above were only achieved for DWRPs due to the ability of delignified wood to be densified. For noninfiltrated DW, an FVC of 70% and above was not obtained due to the spring-back effect, which was observed after densification of oven-dried cellulose scaffolds. The achievable volume fraction of the GFRP was limited due to incompressibility of glass fibers and the type of fabric used. While traditionally, contact of neighboring fibers is not desired, in DWRPs the contact is advantageous because it enhances the interface due to mechanical interlocking of the deformed cells. The deformability enables a closely packed composite with FVCs of above 70%, resulting in materials with remarkably high tensile stiffness of up to 70 GPa and tensile strength of about 600 MPa.

While tensile stiffness (Figure 4a) and tensile strength (Figure 4b) both increase with rising FVC, the increase in stiffness far exceeds predictions from traditional fiber-reinforced composite models, such as the Halpin−Tsai model (see the Supporting Information), which predicts the elasticity of a composite material using the elastic properties of matrix and filler as well as the orientation and geometry of the reinforcing phase.[28] The reported values even exceed the upper limit rule of mixture (ROM, see the Supporting Information)[28] as seen in Figure 4c, assuming an elastic modulus of a single delignified wood fiber of 50 GPa[30,31] and an aspect ratio of 100. A similar trend was found to be true for matrix-free composites,[17] implying that fiber−fiber interactions at high FVCs govern stress transfer ability and allow attainment of mechanical performance exceeding traditional theories.

For observing this effect, high FVCs are needed, which requires a deformable interconnected phase with aligned reinforcing elements. Therefore, delignified wood provides an excellent reinforcing scaffold for high-performance inter-

DOI: 10.1021/acsami.9b11105
ACS Appl. Mater. Interfaces 2019, 11, 35305−35311

penetrating phase composites. Additionally, the low density of cellulose fibers results in high specific tensile properties, and DWRPs with high FVC even outperform all tested reference materials regarding specific tensile properties as shown in Figure 4d and are among the best-performing composites compared to previously reported natural fiber reinforced composites (Figure S5). Tensile elastic moduli, strengths, and densities of DWRPs and reference samples as well as the water uptake of DWRP 70% samples are reported in Table S1. To further study the mechanical behavior of the DWRP composites in a more complex loading environment, bending measurements were conducted.

In bending, the influence of the matrix is even more pronounced, and DWRPs show much higher bending stiffness and strength compared to the noninfiltrated DW (Figure 5, parts a and b), which demonstrates the importance of the interconnected penetrating polymer phase specifically for this loading condition. The DWRP was found to have a similar bending stiffness as GFRP, although the bending strength of GFRP is approximately twice the bending strength of DWRP. This can be explained by analyzing typical stress−strain curves and fractures of 50% FVC samples (Figure S6). The GFRPs show a brittle tensile-dominated failure at 800−900 MPa, whereas DWRPs exhibit strong plastic deformation starting in the range of 100−200 MPa prior to a final fracture around 300 MPa. The DWRP fails in a mixture of compression and tensile failure as shown in the light-microscopy images in Figure S6. Noninfiltrated DW samples failed in compression and showed a plateau at around 100 MPa. Therefore, the interpenetrating matrix stiffens the DW scaffold by filling the empty space in the lumina and helps to resist compression failure at low stress levels. Additionally, interconnections created by infiltrated pits possibly lead to a higher shear modulus and strength that further enhances the structural integrity of the composite material. Due to its lower density, DWRPs outperform GFRPs in terms of specific bending stiffness; however, GFRPs still have a higher specific bending strength compared to the DWRPs. Bending moduli and strengths as well as densities of DWRPs and reference samples are reported in Table S2.

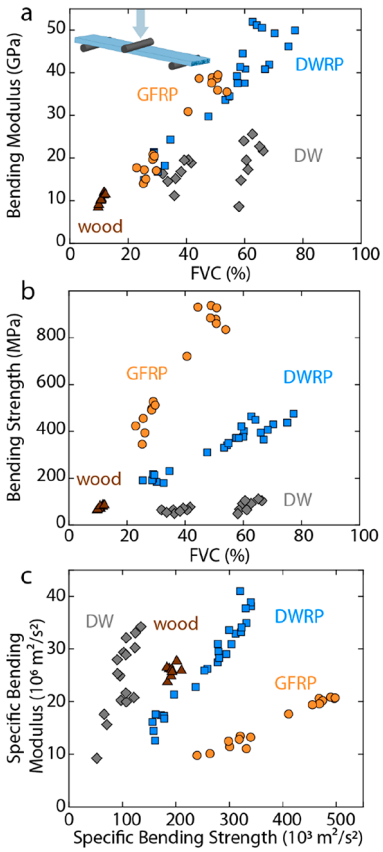

Figure 5. Bending properties of DWRP in comparison to the references native wood, delignified wood (DW), and glass fiber reinforced polymer (GFRP) composites. (a) Bending modulus and (b) bending strength of the composites as a function of their relative FVC. (c) Specific bending modulus vs specific bending strength for the studied composites.

CONCLUSION

We have produced fiber composites showing exceptionally high specific stiffness and strength by the infiltration of epoxy into a wood-derived cellulose scaffold by VARI infiltration followed by densification, achieving FVC of up to 80%. Infiltration in the longitudinal direction is possible due to a percolating porous network inherently present in the preserved delignified wood structure, which exists even after simple air drying of the cellulose scaffold and eliminates the need for elaborate drying techniques such as freeze-drying. The matrix phase creates an interconnected phase, which surrounds the cellulose scaffold that by itself is interconnected forming an interpenetrated composite. The resulting composite possesses very high tensile stiffness and strength of up to 70 GPa and 600 MPa due to a combination of mechanical interlocks between cells, the reinforcing matrix phase connecting fibers through lumen and pits, and a very high FVC of up to 80%. In contrast to synthetic composites, an intimate fiber−fiber contact that allows for very high volume fractions of the reinforcing phase is obtained. This tight contact increases the stress transfer in the composite and leads to an increase in stiffness with FVC, which far exceeds the upper limit ROM. The reported natural fiber composite is in the range of the highest obtained values of wood-based composites using a technique that is fast, efficient, and scalable.

ASSOCIATED CONTENT

Supporting Information

The Supporting Information is available free of charge on the ACS Publications website at DOI: 10.1021/acsami.9b11105.

Image of native wood and partially delignified wood, VARI infiltration setup, densification curves of dry, noninfiltrated cellulose scaffolds at varying wood densities, structural characteristics of DWRPs, comparison of specific tensile properties to literature values, representative tensile stress−strain curves of GFRP, DW, DWRP and wood, light-microscope images of the fracture after bending of GFRP and DWRP, tables with tensile and bending stiffness and strength of all tested materials and of reference material, and Euler's critical load for buckling for earlywood and latewood densification (PDF)

AUTHOR INFORMATION

Corresponding Authors

*E-mail: marionfrey@ethz.ch.
*E-mail: tkeplinger@ethz.ch.

DOI: 10.1021/acsami.9b11105
ACS Appl. Mater. Interfaces 2019, 11, 35305−35311

ORCID

M. Frey: 0000-0002-9242-4331

I. Burgert: 0000-0003-0028-072X

Author Contributions

M.F. and L.S. contributed equally to this work. M.F. designed the study, performed experiments, analyzed data, and cowrote the manuscript; L.S. performed experiments and analyzed data; K.M. designed experiments, analyzed data, and cowrote the manuscript; T.K. analyzed data and cowrote the manuscript; I.B. analyzed data and cowrote the manuscript.

Funding

This work was financed in the framework of the project "Strong Composite" supported under the umbrella of ERA-NET Cofund ForestValue by Innosuisse, AKA, Business Finland, Vinnova, BMLFUW. ForestValue has received funding from the European Union's Horizon 2020 research and innovation programme under Grant Agreement 773324.

Notes

The authors declare no competing financial interest.

■ ACKNOWLEDGMENTS

The authors would like to thank Wilhelm Woigk for the design of the densification mold, Thomas Meierhans for the production of the mold, Thomas Schnider for the preparation of the wood samples, and the Scientific Center for Optical and Electron Microscopy (ScopeM) of ETH for providing the SEM, the ultramicrotome, and their technical support.

■ REFERENCES

(1) Joshi, S. V.; Drzal, L. T.; Mohanty, A. K.; Arora, S. Are Natural Fiber Composites Environmentally Superior to Glass Fiber Reinforced Composites? *Composites, Part A* **2004**, *35* (3), 371−376.

(2) Corbière-Nicollier, T.; Gfeller Laban, B.; Lundquist, L.; Leterrier, Y.; Månson, J.-A.; Jolliet, O. Life Cycle Assessment of Biofibres Replacing Glass Fibres as Reinforcement in Plastics. *Resour., Conserv. Recycl.* **2001**, *33* (4), 267−287.

(3) Mohanty, A. K.; Misra, M.; Drzal, L. T. Sustainable Bio-Composites from Renewable Resources: Opportunities and Challenges in the Green Materials World. *J. Polym. Environ.* **2002**, *10* (1), 19−26.

(4) Berglund, L. A.; Burgert, I. Bioinspired Wood Nanotechnology for Functional Materials. *Adv. Mater.* **2018**, *30* (19), 1704285.

(5) Tingaut, P.; Zimmermann, T.; Sèbe, G. Cellulose Nanocrystals and Microfibrillated Cellulose as Building Blocks for the Design of Hierarchical Functional Materials. *J. Mater. Chem.* **2012**, *22* (38), 20105−20111.

(6) Sehaqui, H.; Allais, M.; Zhou, Q.; Berglund, L. A. Wood Cellulose Biocomposites with Fibrous Structures at Micro- and Nanoscale. *Compos. Sci. Technol.* **2011**, *71* (3), 382−387.

(7) Siqueira, G.; Kokkinis, D.; Libanori, R.; Hausmann, M. K.; Gladman, A. S.; Neels, A.; Tingaut, P.; Zimmermann, T.; Lewis, J. A.; Studart, A. R. Cellulose Nanocrystal Inks for 3D Printing of Textured Cellular Architectures. *Adv. Funct. Mater.* **2017**, *27* (12), 1604619.

(8) Keplinger, T.; Wang, X.; Burgert, I. Nanofibrillated Cellulose Composites and Wood Derived Scaffolds for Functional Materials. *J. Mater. Chem. A* **2019**, *7* (7), 2981−2992.

(9) Frey, M.; Widner, D.; Segmehl, J. S.; Casdorff, K.; Keplinger, T.; Burgert, I. Delignified and Densified Cellulose Bulk Materials with Excellent Tensile Properties for Sustainable Engineering. *ACS Appl. Mater. Interfaces* **2018**, *10* (5), 5030−5037.

(10) Song, J.; Chen, C.; Zhu, S.; Zhu, M.; Dai, J.; Ray, U.; Li, Y.; Kuang, Y.; Li, Y.; Quispe, N.; Yao, Y.; Gong, A.; Leiste, U. H.; Bruck, H. A.; Zhu, J. Y.; Vellore, A.; Li, H.; Minus, M. L.; Jia, Z.; Martini, A.; Li, T.; Hu, L. Processing Bulk Natural Wood into a High-Performance Structural Material. *Nature* **2018**, *554* (7691), 224.

(11) Li, Y. Y.; Fu, Q. L.; Yu, S.; Yan, M.; Berglund, L. Optically Transparent Wood from a Nanoporous Cellulosic Template: Combining Functional and Structural Performance. *Biomacromolecules* **2016**, *17* (4), 1358−1364.

(12) Fu, Q.; Yan, M.; Jungstedt, E.; Yang, X.; Li, Y.; Berglund, L. A. Transparent Plywood as a Load-Bearing and Luminescent Biocomposite. *Compos. Sci. Technol.* **2018**, *164*, 296−303.

(13) Gan, W.; Gao, L.; Xiao, S.; Zhang, W.; Zhan, X.; Li, J. Transparent Magnetic Wood Composites based on Immobilizing Fe3O4 Nanoparticles into a Delignified Wood Template. *J. Mater. Sci.* **2017**, *52* (6), 3321−3329.

(14) Merk, V.; Chanana, M.; Gierlinger, N.; Hirt, A. M.; Burgert, I. Hybrid Wood Materials with Magnetic Anisotropy Dictated by the Hierarchical Cell Structure. *ACS Appl. Mater. Interfaces* **2014**, *6* (12), 9760−9767.

(15) Li, T.; Song, J.; Zhao, X.; Yang, Z.; Pastel, G.; Xu, S.; Jia, C.; Dai, J.; Chen, C.; Gong, A.; Jiang, F.; Yao, Y.; Fan, T.; Yang, B.; Wågberg, L.; Yang, R.; Hu, L. Anisotropic, Lightweight, Strong, and Super Thermally Insulating Nanowood with Naturally Aligned Nanocellulose. *Sci. Adv.* **2018**, *4* (3), eaar3724.

(16) Vidiella del Blanco, M.; Fischer, E. J.; Cabane, E. Underwater Superoleophobic Wood Cross Sections for Efficient Oil/Water Separation. *Adv. Mater. Interfaces* **2017**, *4* (21), 1700584.

(17) Frey, M.; Biffi, G.; Adobes-Vidal, M.; Zirkelbach, M.; Wang, Y.; Tu, K.; Hirt, A. M.; Masania, K.; Burgert, I.; Keplinger, T. Tunable Wood by Reversible Interlocking and Bioinspired Mechanical Gradients. *Adv. Sci.* **2019**, *6* (10), 1802190.

(18) Grönquist, P.; Frey, M.; Keplinger, T.; Burgert, I. Mesoporosity of Delignified Wood Investigated by Water Vapor Sorption. *ACS Omega.* **2019**, *4* (7), 12425−12431.

(19) Navi, P.; Sandberg, D. *Thermo-Hydro-Mechanical Wood Processing*; CRC Press: Boca Raton, FL, 2012.

(20) Yano, H.; Hirose, A.; Collins, P.; Yazaki, Y. Effects of the Removal of Matrix Substances as a Pretreatment in the Production of High Strength Resin Impregnated Wood Based Materials. *J. Mater. Sci. Lett.* **2001**, *20* (12), 1125−1126.

(21) Shams, M. I.; Yano, H. Compressive Deformation of Phenol Formaldehyde (PF) Resin-Impregnated Wood Related to the Molecular Weight of Resin. *Wood Sci. Technol.* **2011**, *45* (1), 73−81.

(22) Yano, H. Potential Strength for Resin-Impregnated Compressed Wood. *J. Mater. Sci. Lett.* **2001**, *20* (12), 1127−1129.

(23) Yano, H.; Hirose, A.; Inaba, S. High-Strength Wood Based Materials. *J. Mater. Sci. Lett.* **1997**, *16* (23), 1906−1909.

(24) Segmehl, J. S.; Studer, V.; Keplinger, T.; Burgert, I. Characterization of Wood Derived Hierarchical Cellulose Scaffolds for Multifunctional Applications. *Materials* **2018**, *11* (4), 517.

(25) Keller, A.; Dransfeld, C.; Masania, K. Flow and Heat Transfer During Compression Resin Transfer Moulding of Highly Reactive Epoxies. *Composites, Part B* **2018**, *153*, 167−175.

(26) Siau, J. F. Permeability. In *Transport Processes in Wood*; Timell, T. E., Ed.; Springer-Verlag: Berlin, Heidelberg, Germany, 1984; pp 73−104.

(27) Brändström, J. Micro-and Ultrastructural Aspects of Norway Spruce Tracheids: A Review. *Iawa J.* **2001**, *22* (4), 333−353.

(28) Matthews, F. L.; Rawlings, R. D. *Composite Materials: Engineering and Science*; CRC Press: Boca Raton, FL, 1999.

(29) Madsen, B.; Thygesen, A.; Lilholt, H. Plant Fibre Composites − Porosity and Volumetric Interaction. *Compos. Sci. Technol.* **2007**, *67* (7), 1584−1600.

(30) Wang, X. Q.; Keplinger, T.; Gierlinger, N.; Burgert, I. Plant Material Features Responsible for Bamboo's Excellent Mechanical Performance: A Comparison of Tensile Properties of Bamboo and Spruce at the Tissue, Fibre and Cell Wall Levels. *Ann. Bot.* **2014**, *114* (8), 1627−1635.

(31) Eichhorn, S.; Baillie, C.; Zafeiropoulos, N.; Mwaikambo, L.; Ansell, M.; Dufresne, A.; Entwistle, K.; Herrera-Franco, P.; Escamilla, G.; Groom, L.; Hughes, M.; Hill, C.; Rials, T. G.; Wild, P. M. Current International Research into Cellulosic Fibres and Composites. *J. Mater. Sci.* **2001**, *36* (9), 2107−2131.

DOI: 10.1021/acsami.9b11105
ACS Appl. Mater. Interfaces 2019, 11, 35305−35311